IJMMM International Journal of Minerals, Metallurgy and Materials 矿物冶金与材料学报（英文版）

Enhanced sulfidization of azurite surfaces by ammonium phosphate and its effect on flotation

Qian Zhang, Shuming Wen, Qicheng Feng, and Han Wang

Cite this article as:
Qian Zhang, Shuming Wen, Qicheng Feng, and Han Wang, Enhanced sulfidization of azurite surfaces by ammonium phosphate and its effect on flotation, *Int. J. Miner. Metall. Mater.*, 29(2022), No. 6, pp. 1150-1160. https://doi.org/10.1007/s12613-021-2379-y

---

International Journal of Minerals, Metallurgy and Materials
Volume 29, Number 6, June 2022, Page 1150
https://doi.org/10.1007/s12613-021-2379-y

Enhanced sulfidization of azurite surfaces by ammonium phosphate and its effect on flotation

Qian Zhang, Shuming Wen, Qicheng Feng✉, and Han Wang

State Key Laboratory of Complex Nonferrous Metal Resources Clean Utilization, Faculty of Land Resource Engineering, Kunming University of Science and Technology, Kunming 650093, China
(Received: 13 August 2021; revised: 28 October 2021; accepted: 8 November 2021)

Abstract: Although azurite is one of the most important copper oxide minerals, the recovery of this mineral via sulfidization–xanthate flotation is typically unsatisfactory. The present work demonstrated the enhanced sulfidization of azurite surfaces using ammonia phosphate ($(NH_4)_3PO_4$) together with Na_2S, based on micro-flotation experiments, time-of-flight secondary ion mass spectrometry (ToF-SIMS), X-ray photoelectron spectroscopy (XPS), zeta-potential measurements, contact angle measurements, Fourier-transform infrared (FT-IR) spectroscopy, and ultraviolet–visible (UV–Vis) spectroscopy. Micro-flotation experiments showed that the floatability of azurite was increased following the simultaneous addition of $(NH_4)_3PO_4$ and Na_2S. ToF-SIMS and XPS analyses demonstrated the formation of a high content of S species on the azurite surface and an increase in the number of Cu(I) species after exposure to $(NH_4)_3PO_4$ and Na_2S, compared with the azurite–Na_2S system. The zeta potential of azurite particles was negatively shifted and the contact angle on the azurite surface was increased with the addition of $(NH_4)_3PO_4$ prior to Na_2S. These results indicate that treatment with $(NH_4)_3PO_4$ enhances the sulfidization of azurite surfaces, which in turn promotes xanthate attachment. FT-IR and UV–Vis analyses confirmed that the addition of $(NH_4)_3PO_4$ increased the adsorption of xanthate with reducing the consumption of xanthate during the azurite flotation process. Thus, $(NH_4)_3PO_4$ has a beneficial effect on the sulfidization flotation of azurite.

Keywords: azurite; ammonium phosphate; enhanced sulfidization; reagent adsorption; flotation enhancement

1. Introduction

Copper is one of the most common nonferrous metals and has numerous applications in various industries and in everyday life because of its unique properties [1–2]. Copper is typically extracted from high-grade sulfide ores, but present-day copper sulfide ore resources are diminishing and new deposits are becoming increasingly difficult to discover. As such, oxide ores and sulfide-oxide mixed ores are being considered as significant future sources of copper [3–4]. Flotation is one of the most common and effective methods of enriching the level of copper minerals in copper oxide ores [5]. These minerals include malachite ($CuCO_3{\cdot}Cu(OH)_2$), azurite ($2CuCO_3{\cdot}Cu(OH)_2$), cuprite (Cu_2O), and chrysocolla ($CuSiO_3{\cdot}2H_2O$). Flotation techniques can be categorized into direct and sulfidization flotation methods, the latter of which is the most widely used for the industrial-scale enrichment of copper oxide ores [6–8].

Sulfidization flotation is also used to process lead oxide and zinc oxide minerals [9–11]. This important process can consist of mechanical, hydrothermal, or surface sulfidization. Surface sulfidization is regarded as an especially effective method because it is inexpensive and readily implemented during industrial production [12–14]. Sodium sulfide (Na_2S) is the most common reagent used to supply S ions [15–16]. Feng *et al.* [17] studied sulfidization flotation using flotation tests, X-ray photoelectron spectroscopy (XPS), zeta-potential measurements, and xanthate adsorption on the surface of malachite to investigate the interaction mechanism of S ions on malachite surfaces. Their study showed that sulfidization pretreatment of malachite before the addition of the xanthate collector improved the floatability of the malachite, as well as the importance of generating specific sulfidization products to enhance the flotation recovery. Lan *et al.* [18] investigated the surface sulfidization of smithsonite by micro-flotation tests, XPS, powder X-ray diffraction (XRD), thermodynamic calculations, and electron-probe microanalysis at high temperatures. Their results showed that a low S concentration can improve the flotation recovery by approximately 65%. Zincite (ZnS and ZnS_2) was formed on the surface of the smithsonite after interaction with sulfide species and these sulfides were distributed over the outer zincite layer. In addition, the average S concentration on the zincite surface increased with the increase in S dosage. The smithsonite surfaces were modified by various S species and the smithsonite flotation recovery was increased after the sulfidization flota-

✉ Corresponding author: Qicheng Feng E-mail: fqckmust@163.com

tion. Even so, it was not possible to collect a large quantity of this valuable mineral during the sulfidization flotation of the oxide ore. Therefore, an activator is needed to enhance the sulfidization of the oxide mineral surfaces and improve recovery [19–21].

Ammonium salts are common activators in industry, and a large amount of research has confirmed that these compounds enhance the flotation recovery of minerals. However, the interaction mechanism has yet to be clarified [22–23]. Shen *et al.* [20] used ammonium phosphate ($(NH_4)_3PO_4$) as an activator to increase the floatability of chrysocolla in sulfidization flotation, and investigated the properties of the chrysocolla surface. Compared with Na_2S–xanthate flotation, the floatability of chrysocolla was greatly improved in the $(NH_4)_3PO_4$–Na_2S–xanthate system because more copper sulfide covered the chrysocolla surfaces, thus improving adsorption of the xanthate. The flotation of malachite with ethanediamine and the associated mechanism have also been investigated [24]. The results demonstrated that, because of the increased formation of copper sulfide species and greater degree of attachment of the collector on the malachite surface, malachite floatability was enhanced by the addition of ethanediamine.

Azurite is an important copper oxide ore and the interactions of azurite with S species have been examined. Specifically, azurite flotation experiments have assessed the effects of the pH of the pulp solution and the Na_2S and xanthate concentrations. Results have indicated that the optimum pH for this process is in the range of 8.5–9.5 and that the use of a suitable sodium sulfide concentration is the key to increasing the flotation recovery of azurite. During a typical flotation process, about 40% of the target minerals are lost in the form of tailings [25–26]. For this reason, NH_4HSO_4 has been employed in the sulfidization flotation of azurite to increase the surface sulfidization, and this technique has been found to enhance sulfidization and improve flotation recovery [27]. In the present work, $(NH_4)_3PO_4$ was examined as an activator to improve azurite floatability. The efficacy of this technique was confirmed by performing micro-flotation experiments and the associated interaction mechanism was analysed using time-of-flight secondary ion mass spectrometry (ToF-SIMS), XPS, Fourier transform infrared (FT-IR) spectroscopy, and ultraviolet–visible (UV–Vis) spectroscopy and elucidated by zeta potential and contact angle measurements.

2. Experimental

2.1. Material and reagents

In preparation for this work, azurite samples were crushed, sieved, and gravity separated. Azurite samples with particle sizes in the range of 37–74 or <37 μm were prepared by grinding and sieving. XRD and chemical multielement analyses confirmed that the samples were highly pure azurite [25]. Deionized water (resistivity: 18.25 MΩ·cm) was employed in all tests of this work. The reagents used in the tests and their purities and functions are summarized in Table 1.

Table 1. Experimental reagents and their functions and purities

Reagent	Function	Purity
Sodium isoamyl xanthate (NaIX, $C_5H_{11}OCSSNa$)	Collector	Commercial grade
Terpenic oil ($C_{10}H_{17}OH$)	Frother	Commercial grade
Hydrochloric acid (HCl)	pH adjustment	Analytical grade
Sodium hydroxide (NaOH)	pH adjustment	Analytical grade
Sodium sulfide ($Na_2S·9H_2O$)	Sulfidization	Analytical grade
Ammonium phosphate ($(NH_4)_3PO_4$)	Enhanced sulfidization	Analytical grade
Sodium chloride (NaCl)	Indifferent electrolyte	Analytical grade

2.2. Micro-flotation experiments

The micro-flotation experiments were carried out in a 40 mL cell, to which a 2-g azurite sample was added together with deionized water. The pH of the resulting dispersion was adjusted to the desired value by the addition of a NaOH solution before any reagents were added. During each trial, $(NH_4)_3PO_4$, $Na_2S·9H_2O$, the xanthate collector, and the frother were added to the dispersion at intervals of 3, 5, 3, and 2 min, respectively, after which the materials that floated or sank in the dispersion were separately gathered, dried, and weighed to calculate the flotation recovery of the azurite.

2.3. Time-of-flight secondary ion mass spectrometry

Azurite samples that had been subjected to different reagent treatments were characterized by ToF-SIMS (ION-TOF GmbH, Münster, Germany). In each case, a bulk azurite sample with a smooth surface was placed in a beaker, to which 100 mL of deionized water was added, with subsequent adjustment of the pH to equal the value used during the corresponding flotation experiment. The flotation reagents $(NH_4)_3PO_4$ and $Na_2S·9H_2O$ were then added sequentially and the dispersion was allowed to stand for 3 and 5 min after each addition, respectively. Each specimen was then allowed to dry in air at room temperature. ToF-SIMS analyses were conducted using 30 keV Bi_3^+ ions at a current of 0.96 pA with an analytical area on the sample surface of 500 μm × 500 μm and a sputter time of 62 s. The positive secondary ion mass spectra were calibrated using C^+, CH_3^+, and $C_4H_9^+$, while the negative secondary ion mass spectra were calibrated using CH^-, $^{37}Cl^-$, and Cu^-.

2.4. X-ray photoelectron spectroscopy

XPS characterization of the samples was performed using

a PHI5000 Versa Probe II instrument (ULVAC-PHI, Japan). In each trial, 1 g of the azurite sample was placed in a beaker and deionized water was added to give a specific concentration, after which the pH was adjusted. After this, the dispersion was treated with various reagents for 15 min each and then repeatedly rinsed with deionized water, followed by solid–liquid separation and drying at room temperature.

2.5. Zeta potential measurements of azurite surfaces

The zeta potentials associated with interactions between the azurite and the reagents were determined using a zeta probe (Zetasizer-3000HS, Malvern Zetasizer Nano ZS90, Malvern Instrument Ltd., United Kingdom). In these experiments, 0.1 g of azurite with particle sizes of <5 μm was dispersed in solution with 100 mL of a 5×10^{-3} mol/L NaCl acting as the electrolyte. Various pH values were used in the different trials. After dispersion of the azurite, $(NH_4)_3PO_4$, $Na_2S{\cdot}9H_2O$, and NaIX were added in order followed by stirring for 3, 5, and 3 min, respectively. The dispersion was subsequently allowed to settle for 10 min, after which a portion of the supernatant was removed for zeta-potential measurements. The final value was obtained by averaging the results from three replicate measurements for each test.

2.6. Contact angle measurements

The floatability of a mineral can be assessed indirectly by measuring the contact angle between the mineral surface and deionized water. In these trials, the surface of the bulk azurite sample was polished, after which the specimen was placed in a beaker containing 50 mL of deionized water at pH of 8.5–9.5. Specific reagents were added to the beaker and allowed to interact with the mineral surface for 3 min. Following this, the azurite was removed from the solution and dried using a rubber suction bulb, after which a JY-82 contact angle analyzer was used to determine the contact angle on the material using the liquid drop method. An image showing the shape of a liquid drop on the sample surface was recorded with a charge-coupled device camera system, and the contact angle was calculated from this image. After this measurement, the sample surface was dried and then polished with abrasive paper to allow for subsequent experiments to assess the contact angles of the azurite after exposure to the other reagents.

2.7. Fourier-transform infrared analysis

FT-IR spectroscopy was used to analyze the chemical compositions of the mineral surface after different reagent treatments. The FT-IR spectra were obtained over the wavenumber range of 600–1200 cm^{-1}. Azurite–Na_2S–NaIX and azurite–$(NH_4)_3PO_4$–Na_2S–NaIX samples were prepared by adding 1 g of azurite to a beaker containing 100 mL deionized water and then adjusting the pH of the dispersion. $(NH_4)_3PO_4$, Na_2S, and xanthate were then added as required and each was allowed to interact with the azurite under ambient conditions for 10 min. Each sample was subsequently removed by filtration, rinsed twice, and air-dried, after which FT-IR spectra were acquired.

2.8. Ultraviolet–visible spectroscopy

The residual xanthate concentrations in the dispersions after reaction of the reagents with the azurite were determined using a UV–Vis spectrophotometer (UV-2007, Shimadzu, Germany). In these experiments, 1 g of azurite was placed in a beaker containing 100 mL deionized water, after which the pH was adjusted. Reagent solutions with the required concentrations were added to this dispersion and the mixtures were stirred for specific time intervals. The solids were then separated from the supernatant by centrifugation.

3. Results and discussion

3.1. Azurite flotation in the presence of $(NH_4)_3PO_4$

Micro-flotation experiments were performed to examine the effect of $(NH_4)_3PO_4$ on the floatability of the azurite. The results (Fig. 1) show that the addition of $(NH_4)_3PO_4$ during the sulfidization process clearly increased the flotation recovery of the azurite (Fig. 1(a)). The azurite recovery was also found to initially increase and then to decrease with the increase in the Na_2S concentration regardless of whether $(NH_4)_3PO_4$ was present (Fig. 1(b)). The use xanthate as the collector is vital to improving the flotation recovery of azurite, and indeed, the floatability of this mineral was increased with the increase in the xanthate concentration (Fig. 1(c)). When only Na_2S was used, a low flotation recovery was obtained, whereas addition of $(NH_4)_3PO_4$ prior to the Na_2S treatment resulted in a greatly increased recovery, providing further evidence for the beneficial effect of $(NH_4)_3PO_4$.

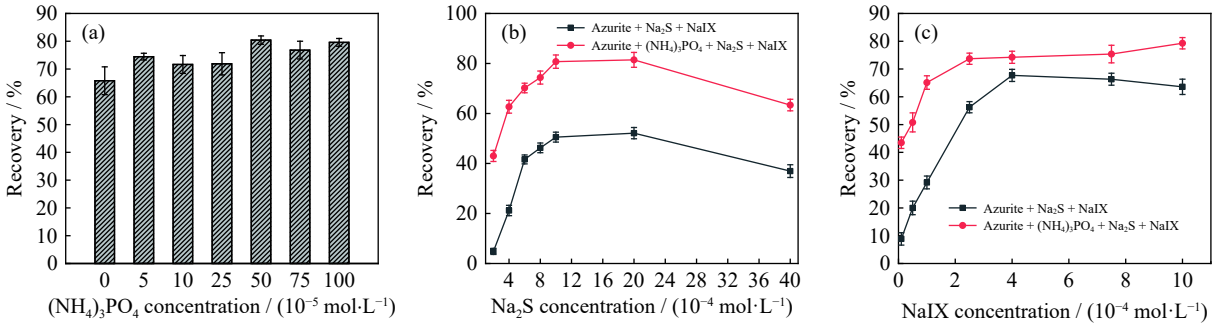

Fig. 1. Flotation recovery of azurite treated with various reagent concentrations: (a) $(NH_4)_3PO_4$; (b) Na_2S, and (c) NaIX (Na_2S: 1×10^{-3} mol/L; $(NH_4)_3PO_4$ and NaIX: 5×10^{-4} mol/L).

3.2. ToF-SIMS

ToF-SIMS was employed to examine changes in the chemical species on the azurite surface following interactions with the various reagents [28–31]. The two-dimensional (2D) distributions of Cu^+, CO_3^-, S^-, S_2^-, CuS_2^-, and SO_3^- ions on the azurite surface after the addition of Na_2S and $(NH_4)_3PO_4$ + Na_2S are shown in Fig. 2(a) and (b), respectively. The distributions of Cu^+, S^-, S_2^-, CuS_2^- and SO_3^- on the azurite surface were notably higher following the $(NH_4)_3PO_4$ + Na_2S treatment than those with direct sulfidization. That is,

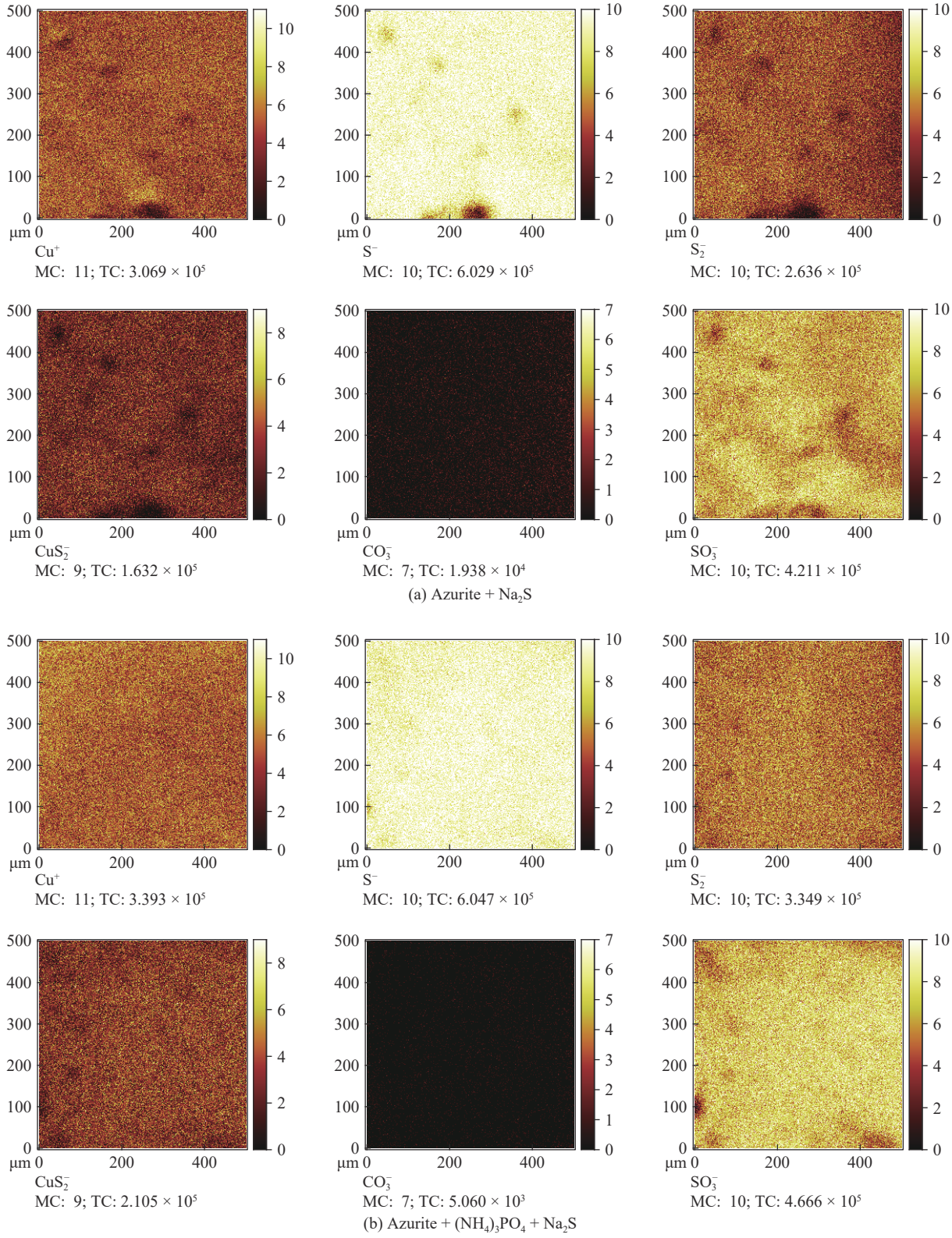

Fig. 2. 2D distributions of the positive and negative ions on the azurite surface following (a) Na_2S and (b) $(NH_4)_3PO_4$ + Na_2S treatments ($(NH_4)_3PO_4$: 5×10^{-4} mol/L; Na_2S: 1×10^{-3} mol/L; MC: Max counts; TC: Total counts).

the intensities of the peaks related to these ions were greater after exposure to the $(NH_4)_3PO_4$ + Na_2S treatment compared with the Na_2S treatment (Fig. 3). This result indicates that the addition of $(NH_4)_3PO_4$ promoted the formation of S species on the azurite surface. Interestingly, a small amount of CO_3^- was distributed on the azurite surface after the Na_2S treatment (Fig. 2(a)), but very little of this ion was present after exposure to the $(NH_4)_3PO_4$ + Na_2S combination (Fig. 2(b)). Specifically, Fig. 3 demonstrates that the CO_3^- peaks (which is related to the degree of sulfidization of the mineral surface) were weak after both the Na_2S and $(NH_4)_3PO_4$ + Na_2S treatments, while the peak intensity was less in the latter case. These data demonstrate that more S species were formed on the azurite surface following exposure to $(NH_4)_3PO_4$ before sulfidization and a greater amount of copper oxide species was transformed to copper sulfide species, thereby increasing the azurite floatability.

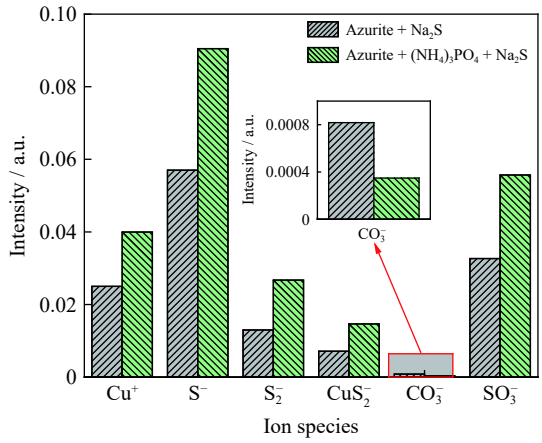

Fig. 3. Intensities of the positive and negative ions on the azurite surface following Na_2S and $(NH_4)_3PO_4$ + Na_2S treatments ($(NH_4)_3PO_4$: 5 × 10^{-4} mol/L; Na_2S: 1 × 10^{-3} mol/L).

3.3. XPS analysis

XPS was used to determine the chemical species and the states of these species on the azurite surface, and thus elucidate the interactions with the different reagents [32–34]. Fig. 4 shows the XPS survey spectra acquired from azurite samples after exposure to the different reagents over the binding energy range of 0–1100 eV. The S peak was generated by the azurite sample after treatment with Na_2S, which shows that sulfide products were generated on the azurite surface. However, the peak intensity was higher after the $(NH_4)_3PO_4$ + Na_2S treatment, compared with the Na_2S treatment, which confirms that more S species were formed. These species increase the hydrophobicity of the azurite surface [35] and thus increase xanthate adsorption to improve the floatability of the azurite.

These spectra were further analyzed by deconvolution and peak fitting, and the contents of C, O, Cu, and S were determined after the effects of carbon impurities were removed (Table 2). The azurite surface exposed to the $(NH_4)_3PO_4$ + Na_2S treatment showed an increase in the Cu content (based on the Cu 2p peak) from 11.03at% to 11.93at% and an increase in the S content (based on the S 2p peak) from 4.67at% to 7.06at%. These data are in accordance with the results in Fig. 4 and indicate that more copper sulfide species were generated on the azurite surface during the $(NH_4)_3PO_4$ + Na_2S treatment than that exposed to only Na_2S.

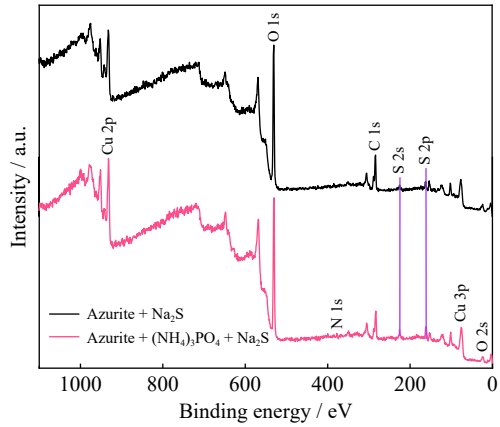

Fig. 4. XPS survey spectra of the azurite surface following Na_2S and $(NH_4)_3PO_4$ + Na_2S treatments ($(NH_4)_3PO_4$: 5 × 10^{-4} mol/L; Na_2S: 1 × 10^{-3} mol/L).

Table 2. Atomic contents on the azurite surface following (a) Na_2S and (b) $(NH_4)_3PO_4$ + Na_2S treatments ($(NH_4)_3PO_4$: 5 × 10^{-4} mol/L; Na_2S: 1 × 10^{-3} mol/L) at%

Sample	C 1s	O 1s	Cu 2p	S 2p
(a)	9.29	75.01	11.03	4.67
(b)	9.52	71.49	11.93	7.06

Peak fitting was applied to the Cu 2p XPS spectra obtained from the azurite surface after the Na_2S and $(NH_4)_3PO_4$ + Na_2S treatments; this process identified two doublet peaks and a pair of satellite peaks (Fig. 5). The peaks with binding energies of 934.84 and 954.74 eV shown in Fig. 5(a) are attributed to Cu(II) species and represent the Cu $2p_{3/2}$ and Cu $2p_{1/2}$ signals, respectively. The peaks at lower binding energies of 932.54 and 952.44 eV are attributed to Cu(I) species [36–37]. Cu(II) species were predominant on the azurite surface, which suggests that Cu(I) had been reduced after exposure to the Na_2S. The data obtained after the $(NH_4)_3PO_4$ + Na_2S treatment (Fig. 5(b)) show a shift in the Cu 2p binding energies. Specifically, the Cu(I) content was increased from 59.75wt% to 63.70wt% with the addition of $(NH_4)_3PO_4$, whereas the concentration of Cu(II) decreased from 40.25wt% to 36.30wt% (Table 3). This result indicates that more S species were generated on the azurite surface together with a higher content of Cu(I) species but fewer Cu(II) species. These changes promote the adsorption of xanthate on the mineral surface, which is consistent with the ToF-SIMS results.

The XPS S 2p spectra obtained from the azurite surface following the Na_2S and $(NH_4)_3PO_4$ + Na_2S treatments were further analyzed and the relative proportions were calculated (Fig. 6 and Table 4, respectively). The S 2p spectrum after the Na_2S treatment shown in Fig. 6(a) exhibits S $2p_{3/2}$ and S $2p_{1/2}$ spin-orbit doublet with an intensity ratio of 2:1 [38]. The

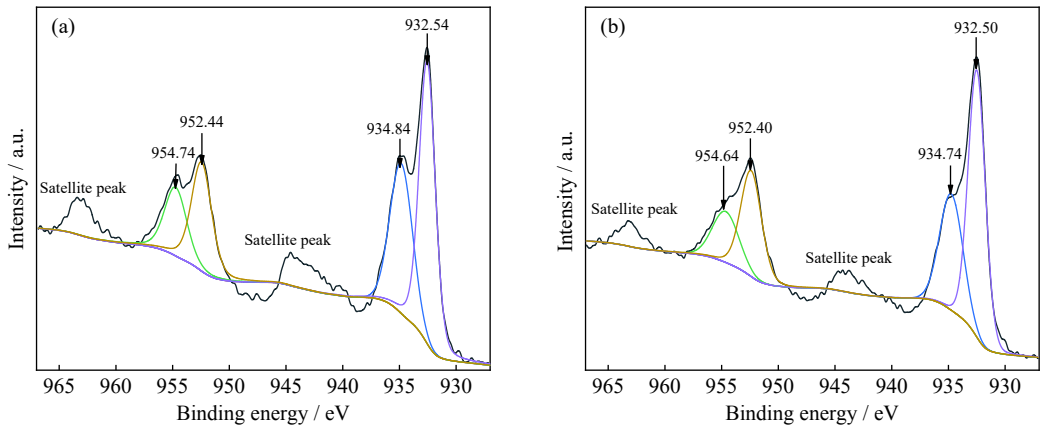

Fig. 5. Cu 2p XPS spectra of the azurite surface following (a) Na_2S and (b) $(NH_4)_3PO_4$ + Na_2S treatments ($(NH_4)_3PO_4$: 5 × 10^{-4} mol/L; Na_2S: 1 × 10^{-3} mol/L).

Table 3. Binding energies and relative Cu proportions based on Cu 2p XPS spectra obtained from the azurite surface following (a) Na_2S and (b) $(NH_4)_3PO_4$ + Na_2S treatments ($(NH_4)_3PO_4$: 5 × 10^{-4} mol/L; Na_2S: 1 × 10^{-3} mol/L)

Sample	Binding energy / eV		Percentage in total Cu / wt%	
	Cu(I)	Cu(II)	Cu(I)	Cu(II)
(a)	932.54	934.84	59.75	40.25
(b)	932.50	934.74	63.70	36.30

three peaks in this spectrum were fitted with binding energies of 161.82, 163.46, and 167.68 eV, which correspond to S^{2-}, S_n^{2-}, and SO_n^{2-}, respectively [39]. That is, monosulfides, polysulfides, and oxysulfides were generated on the azurite surface by exposure to the Na_2S, which would be expected to increase the hydrophobicity of the mineral to improve flotation. The S 2p XPS spectrum of the azurite surface following the addition of $(NH_4)_3PO_4$ + Na_2S (Fig. 6(b)) also confirms the presence of monosulfide, polysulfide, and oxysulfide species. The peak at 161.93 eV was ascribed to monosulfides (S^{2-}), while that at 163.47 eV was attributed to polysulfides (S_n^{2-}). These data suggest that the extent of sulfidization was modified in this case, which would in turn have affected floatability.

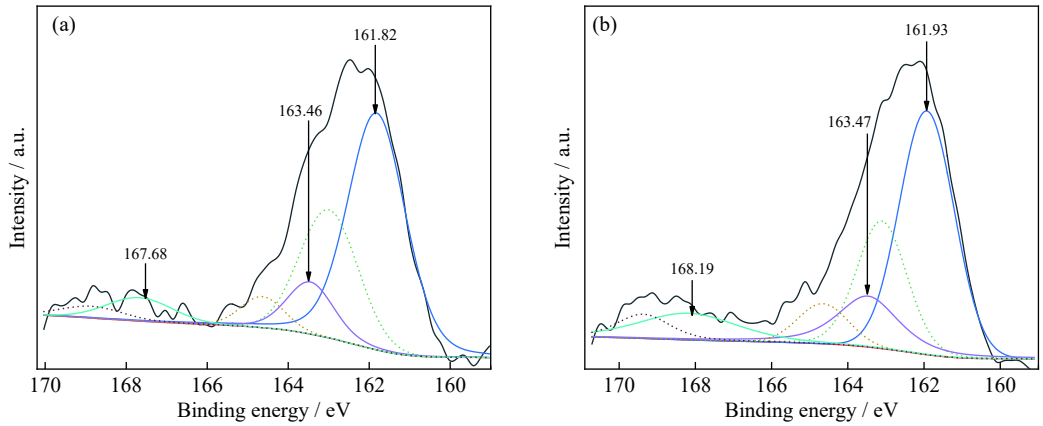

Fig. 6. S 2p XPS spectra obtained from the azurite surface following (a) Na_2S and (b) $(NH_4)_3PO_4$ + Na_2S treatments ($(NH_4)_3PO_4$: 5 × 10^{-4} mol/L; Na_2S: 1 × 10^{-3} mol/L).

Table 4. Binding energies and relative S proportions based on S 2p XPS spectra obtained from the azurite surface following (a) Na_2S and (b) $(NH_4)_3PO_4$ + Na_2S treatments ($(NH_4)_3PO_4$: 5 × 10^{-4} mol/L; Na_2S: 1 × 10^{-3} mol/L)

Sample	Binding energy / eV			Percentage in total S / wt%		
	S^{2-}	S_n^{2-}	SO_n^{2-}	S^{2-}	S_n^{2-}	SO_n^{2-}
(a)	161.82	163.46	167.68	77.52	14.35	8.13
(b)	161.93	163.47	168.19	65.44	19.83	14.73

The relative S contents determined using the S 2p signals obtained from the azurite surface are summarized in Table 4. The percentage of monosulfide species decreased from 77.52wt% to 65.44wt% in the presence of $(NH_4)_3PO_4$ while the proportion of polysulfide species increased from 14.35wt% to 19.83wt%. From these results, it is apparent that more copper polysulfide species were generated on the azurite surface during the $(NH_4)_3PO_4$ + Na_2S treatment. On the basis of these data, we can conclude that $(NH_4)_3PO_4$ generated more sulfidization products on the azurite surface, which

increases the surface hydrophobicity and promotes xanthate adsorption.

3.4. Zeta-potential measurements

The zeta potentials of azurite particles following different reagent treatments were determined to investigate the effect of $(NH_4)_3PO_4$ addition on the adsorption of S ions and xanthate on the azurite surface in the pH range from 5.5 to 11.5. These data are presented in Fig. 7. The results demonstrate that the zeta potential became increasingly negative with gradual increases in pH regardless of the reagents that were used. However, compared with the azurite–Na_2S system, the increased amount of $ROCSS^-$ in the azurite–Na_2S–NaIX system resulted in a more negative zeta potential. The azurite–Na_2S system also showed higher zeta potentials than the azurite–$(NH_4)_3PO_4$–Na_2S system in the pH range from 5.5 to 11.5. More sulfide ions were adsorbed on the azurite surface when $(NH_4)_3PO_4$ was added, which suggests that this compound enhances the sulfidization of the azurite surface. The specimen from the azurite–$(NH_4)_3PO_4$–Na_2S–NaIX surface was found to have a highly negative zeta potential, which indicates that xanthate was adsorbed on the negatively charged azurite surface. Therefore, the addition of $(NH_4)_3PO_4$ increases the flotation recovery of the azurite by enhancing the sulfidization of the azurite surface and increasing the adsorption of the xanthate collector.

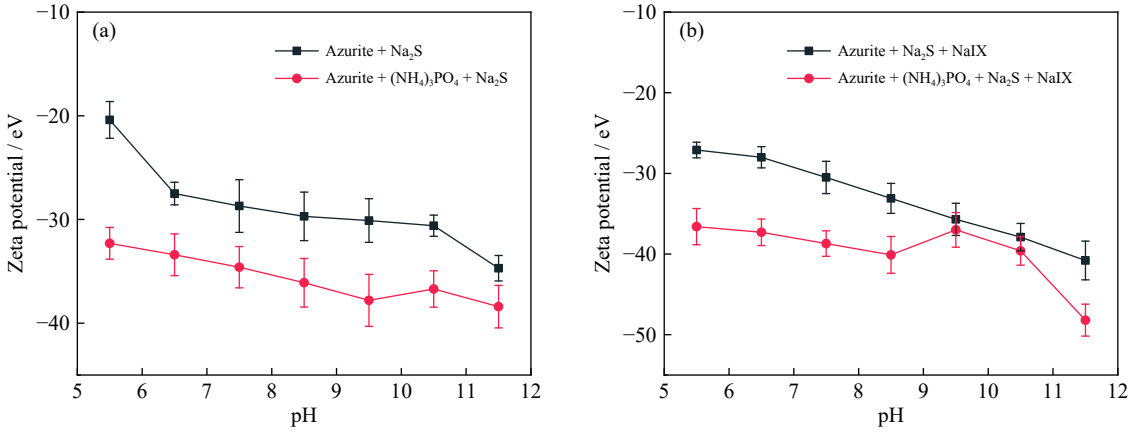

Fig. 7. Zeta potential of azurite as a function of the pH with different flotation reagents: (a) absence of NaIX; (b) presence of NaIX (Na_2S: 1×10^{-3} mol/L; $(NH_4)_3PO_4$ and NaIX: 5×10^{-4} mol/L).

3.5. Contact-angle measurements

The floatability of a mineral is correlated with its hydrophobicity, and the wettability of a mineral surface generally can be assessed on the basis of its contact angle [40–41]. Therefore, the contact angles of azurite surfaces after Na_2S–NaIX and $(NH_4)_3PO_4$–Na_2S–NaIX treatments were determined to characterize the effect of $(NH_4)_3PO_4$ on the azurite floatability during sulfidization at the pH of 8.5–9.5. The resulting contact angles for the Na_2S–NaIX system with different NaIX concentrations and the Na_2S concentration of 1×10^{-3} mol/L are provided in Fig. 8(a). The contact angle increased from 73.74° to 83.97° as the NaIX concentration was increased from 1×10^{-5} to 1×10^{-3} mol/L. In the presence of $(NH_4)_3PO_4$, NaIX concentrations of 1×10^{-5}, 5×10^{-4}, and 1×10^{-3} mol/L gave contact angles of 79.77°, 91.18°, and 93.44°, respectively (Fig. 8(b)). The increase of the contact angle with the increase in the xanthate concentration indicates that the hydrophobicity of the azurite surface was also increased, resulting in improved flotation recovery. In the case of the azurite–Na_2S–NaIX system, the contact angles were small, while 5×10^{-4} mol/L $(NH_4)_3PO_4$ gave a large contact angle. Specifically, the $(NH_4)_3PO_4$ pretreatment increased the contact angles from 73.74°, 81.39°, and 83.97° to 79.77°, 91.18°, and 93.44° for NaIX concentrations of 1×10^{-5}, 5×10^{-4}, and 1×10^{-3} mol/L, respectively. These data show that the $(NH_4)_3PO_4$ pretreatment of the azurite before the addition of Na_2S improved collector attachment to the azurite surface to increase floatability. These phenomena are

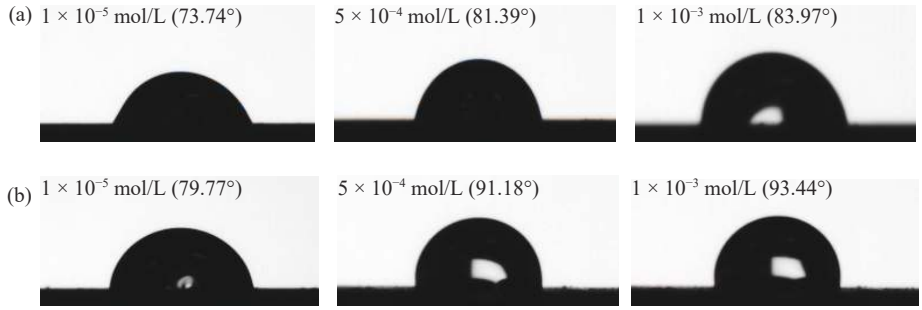

Fig. 8. Contact angles on the azurite surface following (a) Na_2S–NaIX and (b) $(NH_4)_3PO_4$–Na_2S–NaIX treatments using different NaIX concentrations (Na_2S: 1×10^{-3} mol/L; $(NH_4)_3PO_4$: 5×10^{-4} mol/L).

consistent with the results of the micro-flotation experiments.

Fig. 9 provides the contact angles of the azurite surface for different Na_2S concentrations. The contact angle was 73.96° at 2×10^{-4} mol/L Na_2S and 5×10^{-4} mol/L NaIX (Fig. 9(a)), and increasing Na_2S concentration initially increased the contact angle, but then decreased. Similarly, azurite surfaces exposed to the $(NH_4)_3PO_4$–Na_2S–NaIX treatment (Fig. 9(b)) exhibited contact angle first increased but then decreased with the Na_2S concentration raised from 2×10^{-4} to 2×10^{-3} mol/L. It is apparent that the optimal Na_2S concentration improved the azurite flotation. Combining the results shown in Fig. 9(a) and (b), it can be seen that the azurite surface showed a smaller contact angle in the absence of $(NH_4)_3PO_4$, which indicates lower hydrophobicity at a given Na_2S concentration. The addition of $(NH_4)_3PO_4$ before the Na_2S treatment increased the contact angles from 73.96°, 83.76°, and 78.68° to 76.47°, 93.03°, and 89.44° for Na_2S concentrations of 2×10^{-4}, 1×10^{-3}, and 2×10^{-3} mol/L, respectively. The contact angle of the azurite surface treated with $(NH_4)_3PO_4$ before sulfidization was relatively high, which indicates good hydrophobicity, possibly because more copper sulfide was generated on the surface. These contact angle data are in agreement with the results of the micro-flotation experiments.

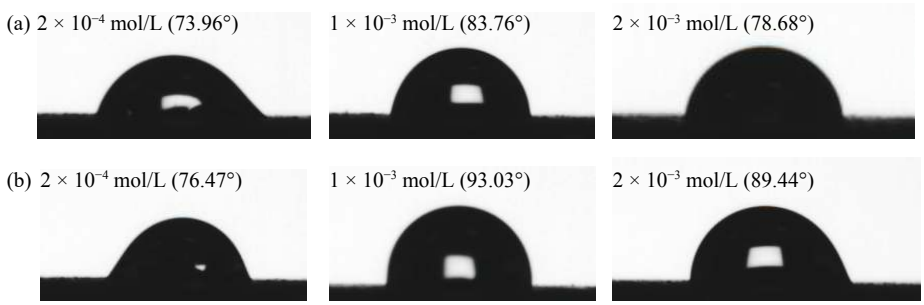

Fig. 9. Contact angles on the azurite surface following (a) Na_2S–NaIX and (b) $(NH_4)_3PO_4$–Na_2S–NaIX treatments using different Na_2S concentrations ($(NH_4)_3PO_4$ and NaIX: 5×10^{-4} mol/L).

3.6. FT-IR and UV–Vis spectroscopy

The interaction between NaIX and the sulfidized azurite was investigated in the presence of $(NH_4)_3PO_4$ by FT-IR and UV–Vis spectroscopy, and the results are shown in Figs. 10 and 11, respectively. The characteristic FT-IR spectrum of the xanthate collector was acquired over the wavenumber range of 600–1200 cm^{-1}. In the FT-IR spectrum of the azurite–Na_2S–NaIX specimen (Fig. 10), the peak at 1091.03 cm^{-1} can be ascribed to the C–O stretching vibration, while that at 1034.62 cm^{-1} may have resulted from the C=S stretching vibration, which suggests interactions between the reagents and azurite surface [42]. The peak at 836.69 cm^{-1} can be attributed to C–H symmetric stretching vibrations and those at 951.43 and 769.45 cm^{-1} correspond to the C–S stretching vibration [43–44]. However, compared with treatment by Na_2S alone, these peaks were shifted in the spectrum of the $(NH_4)_3PO_4$–Na_2S–NaIX system, such that the C–O peak moved from 1091.03 to 1090.06 cm^{-1} and the peak at 1034.62 cm^{-1} shifted to 1033.18 cm^{-1}. These changes demonstrate increased sulfidization of the azurite surface in the presence of $(NH_4)_3PO_4$, possibly because the surface becomes more hydrophobic. In addition, a more intense characteristic peak was obtained from the azurite surface after the $(NH_4)_3PO_4$–Na_2S–NaIX treatment, which indicates that adsorption of xanthate on the azurite surface was enhanced by the addition of $(NH_4)_3PO_4$ before the Na_2S treatment.

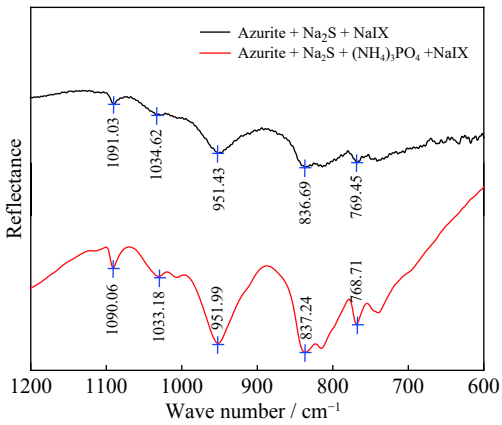

Fig. 10. FT-IR spectra of xanthate adsorbed on the azurite surface following (a) Na_2S and (b) $(NH_4)_3PO_4$–Na_2S treatments.

Because FT-IR showed that the addition of $(NH_4)_3PO_4$ was an important factor enhancing the adsorption of xanthate on the azurite surface, the associated adsorption mechanism was investigated by UV–Vis spectroscopy. The residual xanthate concentrations in the dispersions after azurite interaction with the flotation agents were determined and the uptake of xanthate was calculated (Fig. 11). The data show that increasing the initial xanthate concentration in the dispersion increased the uptake of xanthate by the azurite (Fig. 11(a)). Compared with Na_2S treatment alone, the consumption of xanthate was also increased in the presence of $(NH_4)_3PO_4$, which indicates that more S species have been formed on the azurite surface. Furthermore, uptake of the collector decreased with increasing addition of Na_2S to the azurite–Na_2S system (Fig. 11(b)), which demonstrates that the addition of Na_2S increased the stability of the azurite surface and consequently reduced the surface adsorption of the collector. Furthermore, the consumption of xanthate was lower in the presence of $(NH_4)_3PO_4$, which further verified that $(NH_4)_3PO_4$ increased the extent of sulfidization of the azurite surface

such that the stability of the mineral surface was enhanced during the flotation process. This effect explains the greater flotation recovery obtained after incorporating $(NH_4)_3PO_4$ in the dispersion. The uptake of xanthate increased with the increase in the $(NH_4)_3PO_4$ concentration from 5×10^{-5} to 5×10^{-4} mol/L, although further increase in the amount of $(NH_4)_3PO_4$ had no effect on the consumption of NaIX (Fig. 11(c)). These results confirm that a suitable $(NH_4)_3PO_4$ concentration can enhance the stability of the azurite surface and also decrease the uptake of the xanthate collector. Therefore, we consider that addition of $(NH_4)_3PO_4$ to the pulp solution not only improves the flotation recovery of azurite but also decreases the amount of xanthate that must be used, potentially making the process more economical.

The enhanced sulfidization of the azurite surface by the $(NH_4)_3PO_4$ increased the adsorption of the xanthate collector on the azurite surface, and consequently improved the flotation of the azurite. On the basis of the above data, a model is proposed to explain the enhanced sulfidization obtained by adding $(NH_4)_3PO_4$ during the azurite flotation process (Fig. 12).

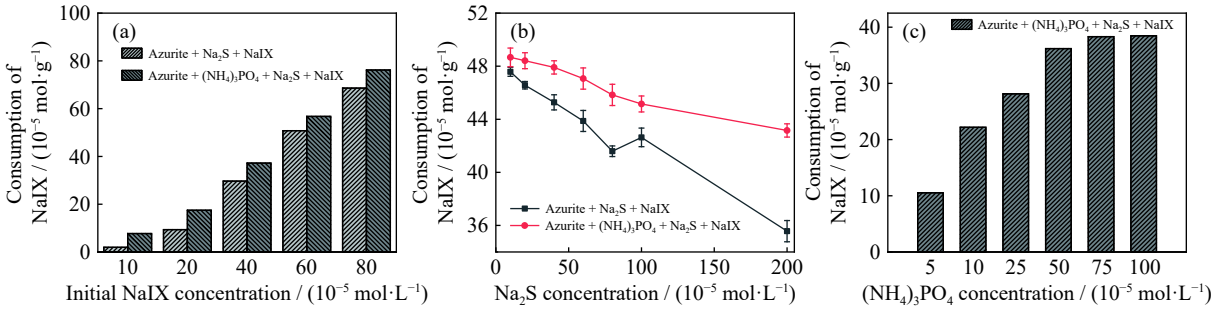

Fig. 11. Consumption of xanthate by azurite surfaces treated with different (a) NaIX, (b) Na_2S, and (c) $(NH_4)_3PO_4$ concentrations (Na_2S: 1×10^{-3} mol/L; $(NH_4)_3PO_4$ and NaIX: 5×10^{-4} mol/L).

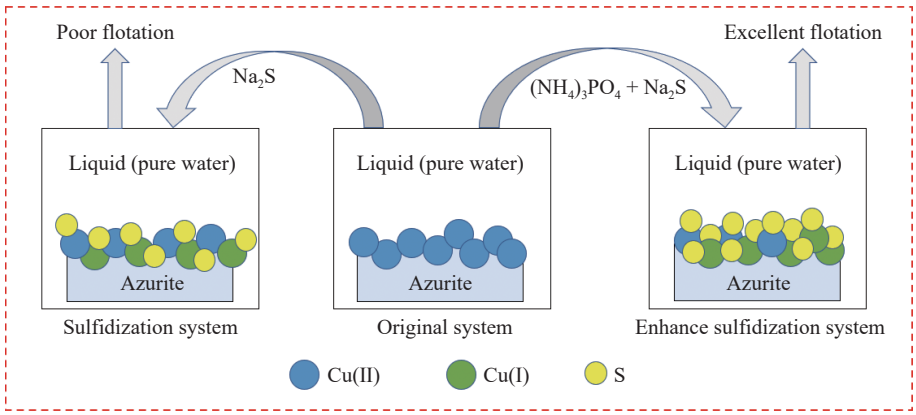

Fig. 12. Diagram showing the enhanced sulfidization of the azurite surface by ammonium phosphate.

4. Conclusion

This work investigated the enhanced sulfidization of the azurite surface obtained by the addition of $(NH_4)_3PO_4$ to the flotation system. Numerous tests and surface analysis methods were used to verify the effect of this reagent during the sulfidization flotation process. The results of micro-flotation experiments indicated that the flotation recovery of azurite increased following the addition of $(NH_4)_3PO_4$. ToF-SIMS and XPS analyses showed that, compared with the azurite + Na_2S system, more sulfide species were generated on the mineral surface in the azurite + $(NH_4)_3PO_4$ + Na_2S system together with a higher content of Cu(I) species, which improved the adsorption of xanthate. Zeta-potential and contact angle measurements confirmed that the incorporation of $(NH_4)_3PO_4$ improved the surface sulfidization of the azurite, thereby increasing the hydrophobicity of the mineral and aiding in flotation recovery. Adsorption experiments showed that the $(NH_4)_3PO_4$ + Na_2S treatment not only increased xanthate adsorption on the azurite surface but also decreased the consumption of the xanthate collector. Hence, surface modification of the azurite by $(NH_4)_3PO_4$ increased the number of copper sites on the azurite surface and formed more CuS species compared with the use of only Na_2S. This interaction promoted further adsorption of the collector and resulted in increased azurite floatability in the azurite + $(NH_4)_3PO_4$ + Na_2S system.

Acknowledgements

This work was supported by the Yunnan Fundamental Research Projects, China (No. 202101BE070001-009) and Ten Thousand Talent Plans for Young Top-notch Talents of Yunnan Province, China (No. YNWR-QNBJ-2018-051).

Conflict of Interest

The authors declare no potential conflicts of interest.

References

[1] S.H. Yin, W. Chen, X.L. Fan, J.M. Liu, and L.B. Wu, Review and prospects of bioleaching in the Chinese mining industry, *Int. J. Miner. Metall. Mater.*, 28(2021), No. 9, p. 1397.

[2] E.B. Moustafa and M.A. Taha, Evaluation of the microstructure, thermal and mechanical properties of Cu/SiC nanocomposites fabricated by mechanical alloying, *Int. J. Miner. Metall. Mater.*, 28(2021), No. 3, p. 475.

[3] H.Y. Xie, Y.H. Liu, B. Rao, J.Z. Wu, L.K. Gao, L.Z. Chen, and X.S. Tian, Selective passivation behavior of galena surface by sulfuric acid and a novel flotation separation method for copper–lead sulfide ore without collector and inhibitor, *Sep. Purif. Technol.*, 267(2021), art. No. 118621.

[4] L.T. Tijsseling, Q. Dehaine, G.K. Rollinson, and H.J. Glass, Flotation of mixed oxide sulphide copper–cobalt minerals using xanthate, dithiophosphate, thiocarbamate and blended collectors, *Miner. Eng.*, 138(2019), p. 246.

[5] X.L. Zhang, J. Kou, C.B. Sun, R.Y. Zhang, M. Su, and S.F. Li, Mineralogical characterization of copper sulfide tailings using automated mineral liberation analysis: A case study of the Chambishi Copper Mine tailings, *Int. J. Miner. Metall. Mater.*, 28(2021), No. 6, p. 944.

[6] G.R. Wang, H.Y. Yang, Y.Y. Liu, L.L. Tong, and A. Auwalu, Study on the mechanical activation of malachite and the leaching of complex copper ore in the Luanshya mining area, Zambia, *Int. J. Miner. Metall. Mater.*, 27(2020), No. 3, p. 292.

[7] W.Z. Yin and Y. Tang, Interactive effect of minerals on complex ore flotation: A brief review, *Int. J. Miner. Metall. Mater.*, 27(2020), No. 5, p. 571.

[8] G. Han, S.M. Wen, H. Wang, and Q.C. Feng, Sulfidization regulation of cuprite by pre-oxidation using sodium hypochlorite as an oxidant, *Int. J. Min. Sci. Techno.*, 31(2021), No. 6, p. 1117.

[9] J.P. Cai, D.W. Liu, P.L. Shen, X.L. Zhang, K.W. Song, X.D. Jia, and C. Su, Effects of heating-sulfidation on the formation of zinc sulfide species on smithsonite surfaces and its response to flotation, *Miner. Eng.*, 169(2021), art. No. 106956.

[10] J.L. Li, S.Y. Liu, D.W. Liu, R.Z. Liu, Z.C. Liu, X.D. Jia, and T.C. Chang, Sulfidization mechanism in the flotation of cerussite: A heterogeneous solid–liquid reaction that yields $PbCO_3$/PbS core–shell particles, *Miner. Eng.*, 153(2020), art. No. 106400.

[11] C. Liu, G.L. Zhu, S.X. Song, and H.Q. Li, Interaction of gangue minerals with malachite and implications for the sulfidization flotation of malachite, *Colloids Surf. A*, 555(2018), p. 679.

[12] Z. Li, M. Chen, P.W. Huang, Q.W. Zhang, and S.X. Song, Effect of grinding with sulfur on surface properties and floatability of three nonferrous metal oxides, *Trans. Nonferrous Met. Soc. China*, 27(2017), No. 11, p. 2474.

[13] X.B. Min, C.Y. Yuan, Y.J. Liang, L.Y. Chai, and Y. Ke, Metal recovery from sludge through the combination of hydrothermal sulfidation and flotation, *Procedia Environ. Sci.*, 16(2012), p. 401.

[14] D.D. Wu, Y.B. Mao, J.S. Deng, and S.M. Wen, Activation mechanism of ammonium ions on sulfidation of malachite (-201) surface by DFT study, *Appl. Surf. Sci.*, 410(2017), p. 126.

[15] D.Q. Xing, Y.Q. Huang, C.S. Lin, W.R. Zuo, and R.D. Deng, Strengthening of sulfidization flotation of hemimorphite via fluorine ion modification, *Sep. Purif. Technol.*, 269(2021), art. No. 118769.

[16] R.Z. Liu, D.W. Liu, J.L. Li, S.Y. Liu, Z.C. Liu, L.Q. Gao, X.D. Jia, and S.F. Ao, Improved understanding of the sulfidization mechanism in cerussite flotation: An XPS, ToF-SIMS and FESEM investigation, *Colloids Surf. A*, 595(2020), art. No. 124508.

[17] Q.C. Feng, W.J. Zhao, S.M. Wen, and Q.B. Cao, Copper sulfide species formed on malachite surfaces in relation to flotation, *J. Ind. Eng. Chem.*, 48(2017), p. 125.

[18] Z.Y. Lan, Z.N. Lai, Y.X. Zheng, J.F. Lv, J. Pang, and J.L. Ning, Thermochemical modification for the surface of smithsonite with sulfur and its flotation response, *Miner. Eng.*, 150(2020), art. No. 106271.

[19] Q.C. Feng, W.J. Zhao, and S.M. Wen, Ammonia modification for enhancing adsorption of sulfide species onto malachite surfaces and implications for flotation, *J. Alloys Compd.*, 744(2018), p. 301.

[20] P.L. Shen, D.W. Liu, X.H. Xu, X.D. Jia, X.L. Zhang, K.W. Song, and J.P. Cai, Effects of ammonium phosphate on the formation of crystal copper sulfide on chrysocolla surfaces and its response to flotation, *Miner. Eng.*, 155(2020), art. No. 106300.

[21] S.J. Bai, C.L. Li, X.Y. Fu, Z. Ding, and S.M. Wen, Promoting sulfidation of smithsonite by zinc sulfide species increase with addition of ammonium chloride and its effect on flotation performance, *Miner. Eng.*, 125(2018), p. 190.

[22] X. Bai, J. Liu, S.M. Wen, Y. Wang, and Y.L. Lin, Effect of ammonium salt on the stability of surface sulfide layer of smithsonite and its flotation performance, *Appl. Surf. Sci.*, 514(2020), art. No. 145851.

[23] P.L. Shen, D.W. Liu, X.L. Zhang, X.D. Jia, K.W. Song, and D. Liu, Effect of $(NH_4)_2SO_4$ on eliminating the depression of excess sulfide ions in the sulfidization flotation of malachite, *Miner. Eng.*, 137(2019), p. 43.

[24] Q.C. Feng, W.J. Zhao, and S.M. Wen, Surface modification of malachite with ethanediamine and its effect on sulfidization flotation, *Appl. Surf. Sci.*, 436(2018), p. 823.

[25] Q. Zhang, Y.J. Wang, Q.C. Feng, S.M. Wen, Y.W. Zhou, W.L. Nie, and J.B. Liu, Identification of sulfidization products formed on azurite surfaces and its correlations with xanthate adsorption and flotation, *Appl. Surf. Sci.*, 511(2020), art. No. 145594.

[26] Q. Zhang, S.M. Wen, Q.C. Feng, and S. Zhang, Surface characterization of azurite modified with sodium sulfide and its response to flotation mechanism, *Sep. Purif. Technol.*, 242(2020), art. No. 116760.

[27] Q.Y. Sheng, W.Z. Yin, B. Yang, S.H. Cao, H.R. Sun, Y.Q. Ma, and K.Q. Chen, Improving surface sulfidization of azurite with ammonium bisulfate and its contribution to sulfidization flotation, *Miner. Eng.*, 171(2021), art. No. 107072.

[28] M. Finšgar, Surface analysis by gas cluster ion beam XPS and ToF-SIMS tandem MS of 2-mercaptobenzoxazole corrosion inhibitor for brass, *Corros. Sci.*, 182(2021), art. No. 109269.

[29] H. Lai, J.S. Deng, Q.J. Liu, S.M. Wen, and Q. Song, Surface chemistry investigation of froth flotation products of lead–zinc sulfide ore using ToF-SIMS and multivariate analysis, *Sep. Purif. Technol.*, 254(2021), art. No. 117655.

[30] H. Lai, Q.J. Liu, J.S. Deng, S.M. Wen, and Z.L. Liu, Surface chemistry study of Cu–Pb sulfide ore using ToF-SIMS and multivariate analysis, *Appl. Surf. Sci.*, 518(2020), art. No. 146270.

[31] S.J. Bai, P. Yu, Z. Ding, Y.X. Bi, C.L. Li, D.D. Wu, and S.M. Wen, New insights into lead ions activation for microfine particle ilmenite flotation in sulfuric acid system: Visual MINTEQ models, XPS, and ToF-SIMS studies, *Miner. Eng.*, 155(2020), art. No. 106473.

[32] V.S.G. Krishna and M.G. Mahesha, XPS analysis of $ZnS_{0.4}Se_{0.6}$ thin films deposited by spray pyrolysis technique, *J. Electron Spectrosc. Relat. Phenom.*, 249(2021), art. No. 147072.

[33] B.V. Crist, The XPS library website: A resource for the XPS community including - The XPS library of information, XPS spectra-base having >70,000 monochromatic XPS spectra, and spectral data processor (SDP) v8.0 software, *J. Electron Spectrosc. Relat. Phenom.*, 248(2021), art. No. 147046.

[34] Y. Kubo, Y. Sonohara, and S. Uemura, Changes in the chemical state of metallic Cr during deposition on a polyimide substrate: Full soft XPS and ToF-SIMS depth profiles, *Appl. Surf. Sci.*, 553(2021), art. No. 149437.
[35] G. Han, S.M. Wen, H. Wang, and Q.C. Feng, Surface sulfidization mechanism of cuprite and its response to xanthate adsorption and flotation performance, *Miner. Eng.*, 169(2021), art. No. 106982.
[36] H.Q. Peng, D. Wu, and M. Abdelmonem, Flotation performances and surface properties of chalcopyrite with xanthate collector added before and after grinding, *Results Phys.*, 7(2017), p. 3567.
[37] G. Han, S.M. Wen, H. Wang, and Q.C. Feng, Effect of ferric ion on cuprite surface properties and sulfidization flotation, *Sep. Purif. Technol.*, 278(2021), art. No. 119573.
[38] C.L. Li, S.J. Bai, Z. Ding, P. Yu, and S.M. Wen, Visual MINTEQ model, ToF-SIMS, and XPS study of smithsonite surface sulfidation behavior: Zinc sulfide precipitation adsorption, *J. Taiwan Inst. Chem. Eng.*, 96(2019), p. 53.
[39] J.J. Luo, Q. Niu, M.C. Jin, Y.N. Cao, L.R. Ye, and R.P. Du, Study on the effects of oxygen-containing functional groups on Hg^0 adsorption in simulated flue gas by XAFS and XPS analysis, *J. Hazard. Mater.*, 376(2019), p. 21.
[40] S. Krainer and U. Hirn, Contact angle measurement on porous substrates: Effect of liquid absorption and drop size, *Colloids Surf. A*, 619(2021), art. No. 126503.
[41] G. Huminic, A. Huminic, F. Dumitrache, C. Fleaca, and I. Morjan, Experimental study on contact angle of water based Si–C nanofluid, *J. Mol. Liq.*, 332(2021), art. No. 115833.
[42] Y.J. Yang, L.Y. Zhang, Y.L. Zhu, G.T. Wei, Z.M. Li, and R.L. Mo, Three-dimensional photoelectrocatalytic degradation of ethyl xanthate catalyzed by activated bentonite-based bismuth ferrites particle electrodes: Influencing factors, kinetics, and mechanism, *J. Environ. Chem. Eng.*, 9(2021), No. 4, art. No. 105559.
[43] G.C. Zhu, J.F. Liu, J. Yin, Z.W. Li, B.Z. Ren, Y.J. Sun, P. Wan, and Y.S. Liu, Functionalized polyacrylamide by xanthate for Cr(VI) removal from aqueous solution, *Chem. Eng. J.*, 288(2016), p. 390.
[44] Z.L. Li, Y. Kong, and Y.Y. Ge, Synthesis of porous lignin xanthate resin for Pb^{2+} removal from aqueous solution, *Chem. Eng. J.*, 270(2015), p. 229.